Acta Cryst. (1960). **13**, 205

Automatic Single Crystal Diffractometry. I. The Kinematic Problem

By J. Ladell and K. Lowitzsch

Philips Laboratories, Irvington-on-Hudson, New York, U.S.A.

(*Received* 27 *May* 1959 *and in revised form* 20 *July* 1959)

Counter and crystal motions are coupled to explore the reflection space of a crystal along parallel lines in the reciprocal lattice by utilizing any one of three mechanical linkage mechanisms that are described here. The kinematic relations among the moving elements of each of the mechanisms are derived. These relations are used to evaluate the feasibility of these mechanisms as bases for automatic diffractometers.

1. Introduction

The need for efficient automatic counter devices for single crystal structure analysis has been acute for some time. Crystallographers are presently focusing their attention on crystals of larger cell dimensions, electronic computers are being utilized to facilitate the refinement of structural parameters, impetus has been given to statistical procedures for phase determinations, and the exploitation of anomalous dispersion has been recently innovated (Okaya, Saito & Pepinsky, 1955) for the solution of non-centrosymmetric crystal structures. However, the experimental methods of obtaining intensity data have not kept pace with these elegant systems and enterprises for the reduction or interpretation of the data. As attention is turned to the elucidation of the structural properties of molecules of ever increasing complexity, the experimental task of recording densely populated reciprocal lattices has become enormously time-consuming. Crystallographers often have been compelled to limit their objectives, and in many cases sacrifice quality for quantity to accumulate the prodigious amount of data.

Now that the use of large computers has enhanced the refinement of structural problems, the need for more accurate intensity data is more acutely sensed. Aside from the general solution of the phase problem, the acquisition of accurate intensity data remains one of the most important problems in X-ray crystallography.

The utilization of modern counter detectors for the acquisition of single crystal intensity data has been advocated for some time, and the technology of counter devices used for X-ray work has reached an advanced stage. The counter detector has been employed extensively in powder diffractometry (Parrish, Hamacher & Lowitzsch, 1954; Parrish & Kohler, 1956), and its use for single crystal applications has received considerable attention. The adaptation of a Geiger–Mueller counter to the Weissenberg camera was implemented in several designs such as those by Clifton, Fuller & McLachlan (1951), and Evans (1953). A comprehensive evaluation of the measurement of Bragg and diffuse scattering using a Geiger–Mueller counter was conducted by Lonsdale (1948). Improved Geiger–Mueller techniques including consideration of the balanced filter method, monochromatization and a study of counting statistics were reported by Cochran (1950).

Some of the difficulties facing the early users of the Geiger–Mueller counter have been overcome by the development of proportional and scintillation counters. Thus, the non-linear response of the Geiger counter and its choking at high counting rates are partially overcome by the use of the proportional counter and the NaI scintillation counter (Parrish & Kohler, 1956). The high quantum counting efficiency of the latter for short wavelength X-rays makes it particularly useful for single crystal work. The use of energy discrimination to remove subharmonic wavelength components of the diffracted intensity has eliminated one of the serious deficiencies that limited the range of the earlier counter techniques.

In formulating the geometrical problems specifically associated with the use of counters, Hirshfeld & Schmidt (1953) clearly pointed out some of the disadvantages that arise because the counter, essentially a local detector, can measure only one reflection at a time. The accurate placement of the counter in position to detect correctly the integrated intensity from an individual reflection must be repeated for each of the numerous reflections. In addition, recognizing that the feasibility of single crystal counter techniques would be enhanced by adopting a general scanning procedure, Hirshfeld & Schmidt (1953) were first to advocate a scanning procedure based upon the exploration of the reciprocal lattice along parallel reciprocal lattice lines, and to realize that the motion required to accomplish this mode of exploration was mechanically feasible.

No experimentally defined incident X-ray beam meets the ideal conditions set forth in the strict definition of 'integrated intensity'. In film techniques, the error in determining the experimental structure factors from (oftentimes visual) estimates of the blackening of diffraction spots in photographic emul-

sions generally masks any error due to the lack of definition of the spectral composition of the spot. A realistic definition of integrated intensity requires that the spectral composition be the same for each reflection measured. In the estimation of film intensities it is practically impossible to delineate a uniform spectral breadth for all reflections, and therefore visual and photometric integration schemes employed must be of limited accuracy. The spectral distribution of each reflection is easily discerned with proper counter techniques because complete line profiles (spectral distributions) can be measured. Thus, by providing an incident beam which is severely restricted in its spectral composition, uniform spectral composition in each detected reflection can be assured, and, thereby, a considerable improvement in accuracy can be attained in the measurement of integrated intensities. Methods for controlling the spectral composition of the incident beam through the use of crystal monochromators, the attendant geometrical problems that the use of such high resolution devices imposes, and the theoretical problems associated with the spectral composition of single crystal diffraction effects will be discussed in a separate paper.

In automatic diffractometry where the objective is primarily accurate intensity measurements, the employment of spherical or cylindrically shaped 'study' crystals is virtually mandatory if a satisfactory account is to be given for the effect of absorption. Such restrictions on the study crystal limit the applicability of well known procedures for the initial alignment of crystals and require that in an automatic diffractometer there be a feature of design that permits alignments to be made exclusively by X-ray methods.

In order that the crystal be exposed to the identical incident beam cross-section (particularly when monochromatized X-rays are used) regardless of the angular orientation to which it is brought, the crystal centering tolerances as well as the stability of the crystal axis of rotation must be maintained to more precise tolerances than are requisite in the film devices. Errors due to these aberrations, though not observed in film technology, are readily detected with sensitive counter detectors.

The problems mentioned here relating to the employment of a counter detector in single crystal automatic diffractometry fall into two categories. In the first category, we have problems that arise because of the high efficiency and extreme sensitivity of the counter detector. To realize the full potential of the counter as a device for *accurate* intensity measurement, it is necessary to give serious attention to these problems which are generally ignorable in film work, since in film work these aberrations are not the principle sources of inaccuracy. (For example, a mechanically unstable crystal axis of rotation which causes a 2% error in the integrated intensity is not a serious problem when the spot on the film cannot be read to better than 15%.) In the second category we have problems that arise specifically because of the local nature of the detector—its inability to simultaneously distinguish spatially separated events. Unlike the film detector, which detects over an area, the counter is a point detector.

The role of the problems of the first category in relation to the design of an automatic single crystal diffractometer of high precision will be discussed in more detail in a separate paper. This paper is concerned with the problems of the second category, namely, the kinematic aspects of automatic diffractometry, the tracking of the counter motion with that of the crystal motion in order that the reciprocal lattice be rapidly explored and the reflections efficiently scanned.

2. The kinematic problem

In order to explore or scan continuously along a specified reciprocal lattice line by means of a counter detector adaptation of the equi-inclination Weissenberg technique, a mechanism is required that constrains the counter detector to conform to the tracking equation

$$Y = \omega \pm \cos^{-1}(\cos\omega + g)\,, \tag{1}$$

where Y is the counter angle, i.e., the angle between the incident X-rays and the direction of the projection of the counter arm in the plane of the zero-level of the reciprocal lattice of the study crystal. The crystal angle, ω, is the angle between the specified reciprocal lattice line and the normal (which passes through the specified reciprocal lattice line) to the plane defined by the crystal axis of rotation and the incident X-ray beam. g is defined by

$$g = v/\cos\nu\,, \tag{2}$$

where v is the distance from the specified reciprocal lattice line to the axis of rotation of the reciprocal lattice, and ν is the equi-inclination angle.

Equation (1) has been derived by Buerger (1942), who used other symbols for Y and g; the derivation can be easily understood by referring to his Figs. 139 and 146*A*. Fig. 1 shows part of Buerger's construction in our nomenclature. In Fig. 1(*a*) the orthogonal reciprocal lattice lines $\overline{PP'}$ and $\overline{QQ'}$ define an nth reciprocal lattice level. Q is the intersection of the circle of reflection for that level with the plane which contains the incident X-ray beam and is normal to the reciprocal lattice level. $\overline{T'O}$ and $\overline{TO}$ are the two counter arm projections in the level and they determine the (counter) angles Y and Y', respectively. The crystal angle, ω, is the angle between $\overline{ZQ}$ (the normal to $\overline{OQ}$) and the specified reciprocal lattice line $\overline{PP'}$. u_1 and u_2 are the reflecting positions on the line $\overline{PP'}$ and v is the distance from $\overline{PP'}$ to Q. $\overline{RR'}$ is the direction of the projection of the X-ray beam in the

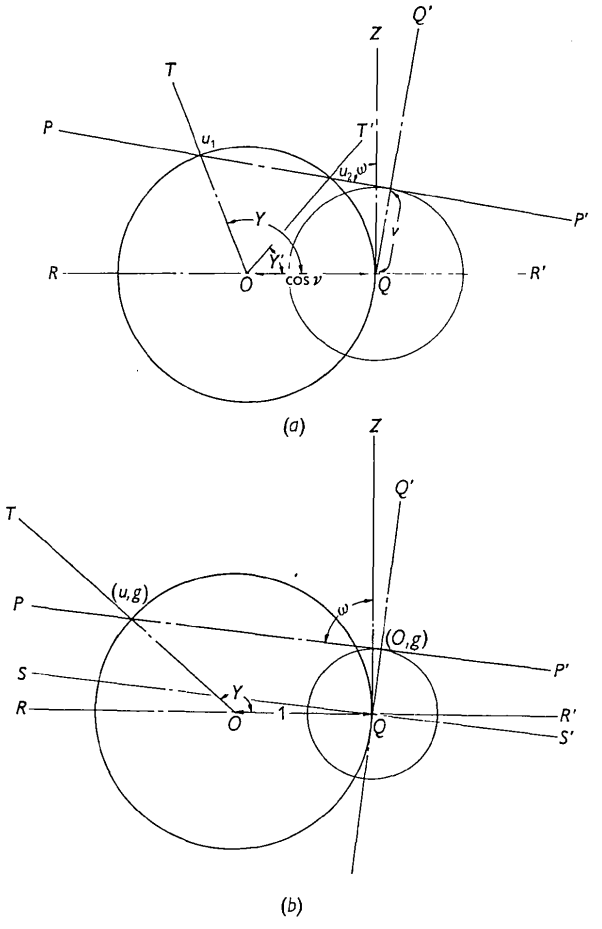

Fig. 1. (*a*) Geometric construction for derivation of tracking equation (1). $\overline{TO}$ and $\overline{TO'}$ are the directions along which two counter detectors can be placed to detect diffraction effects occurring at u_1 and u_2 on the circle of reflection. (*b*) Geometric construction for one counter arrangement. The scale of the drawing is such that the intercept of the sphere of reflection with the nth level, i.e., the circle of reflection for the nth level in the equi-inclination scheme, has unit radius. $\overline{SS'}$ and $\overline{QQ'}$ are coordinate axes with reference to which the point (u, g) can be located in the reciprocal lattice level.

plane of the reciprocal lattice level. The radius of the circle of reflection $\overline{OQ}$ is equal to $\cos \nu$. The circle about Q of radius v is the locus of the intersection of $\overline{PP'}$ and $\overline{QQ'}$ as the crystal is rotated.

The problem is to couple the motions of the counter detector and the crystal rotation in order to move the point u_1 and/or u_2 along the reciprocal lattice line $\overline{PP'}$ so that the reflecting condition is maintained and the counter is at the same time properly oriented to detect the diffraction effects. We have investigated several schemes for mechanical coupling and these are reported here. In treating this problem from the mechanical point of view, we differ from the approaches of Bond (1955), and that of Pepinsky, Diamant & Drenck (1959). In the Bond approach, which is essentially electronic, the counter detector is applied in a method analogous to the systematic photometry of a Weissenberg film. In the approach of Pepinsky *et al.* (1959), the coupling is electrical, i.e., the motions of the counter and crystal are servocontrolled by resolvers which convert electrical resistances into angular deflections; the angular deflections in turn are transferred by means of servo motors to counter and crystal angular deflections. Although the methods of Bond (1955) and of Pepinsky *et al.* (1959) represent advances in the technique of automatic diffractometers, we feel that the mechanical approach is not only more direct but also offers the most promising possibilities with respect to the attainment of high precision in the experimental processes for crystal structure determination. Mathiesen (1958) has given a description of one type of mechanical linkage. An automatic diffractometer for neutron diffraction has been designed by Langdon & Frazer (1959); it is electro-mechanically controlled by Digitizers.

It is convenient for the discussion that follows to distinguish between 'scanning' and 'exploring' along a given path in the reciprocal lattice. 'Scanning' is used to denote the deliberate systematic examination of the diffraction effect in the vicinity of a reciprocal lattice point and 'exploration' is reserved for searching or traversing a given path without necessarily recording any diffraction effects that may be encountered. The distinction between these two processes in automatic diffractometry is apparent when it is recognized that useful diffraction data are generally available only at sites in the reciprocal lattice where there are reciprocal lattice points. In certain applications, e.g., the study of temperature diffuse scattering, the regions between reflections may be of paramount interest.

It is clear from (1) and Fig. 1(*a*) that exploration along the line $\overline{PP'}$ can be accomplished by a mechanical linkage utilizing two counters simultaneously. Although this scheme is feasible it was ruled out as not being sufficiently advantageous to warrant the additional complications that would arise from the second counter and the involved electronic circuitry. In developing a mechanical method for executing the exploration, we have accordingly restricted our attention to the use of one counter and have studied methods of providing a mechanical analog solution to the tracking equation,

$$Y = \omega + \cos^{-1}(\cos \omega + g) \,. \qquad (3)$$

Three mechanical arrangements were considered feasible, and these were systematically investigated to evaluate their potential as the basis for an automatic diffractometer. We were governed by two important considerations: (*a*) It should be possible to easily implement the linkage mechanism with devices to provide for a completely automated system for obtaining the data of a zone or (upper) level of reflections. (*b*) The analog solution of (3) should be obtained with high precision. The various mechanisms, cate-

gorized by the element of the linkage that receives the primary motion, are: the counter drive, the crystal drive, and the point drive.

The essential construction for a one-counter linkage is shown in Fig. 1(*b*). The scale of the circle of reflection for the *n*th level has been altered in such a manner as to essentially preserve the construction of Fig. 1(*a*). The radius of the circle of reflection in Fig. 1(*b*) is drawn $\overline{OQ}=1$. Ewald's construction is preserved by increasing the dimensions of the reciprocal lattice by the factor $1/\cos\nu$. Thus the distance v shown in Fig. 1(*a*) is replaced by the (scaled) distance g in Fig. 1(*b*). (The maintenance of a unit circle of reflection for all levels is a normalization which anticipates the foregoing description of mechanical analogs for the construction of Fig. 1(*a*).) In this construction $\overline{QQ'}$ and $\overline{SS'}$ are orthogonal coordinate axes that intersect at $Q(0, 0)$. The common point of intersection of the circle of reflection (radius $\overline{OQ}$), $\overline{TO}$ and $\overline{PP'}$ has the coordinates (u, g).

In terms of the coordinates (u, g),

$$Y=2\sin^{-1}[(u^2+g^2)^{\frac{1}{2}}/2]\,. \tag{4}$$

To specify the crystal angle ω in terms of (u, g), it is convenient to define a term β where

$$\beta=[4(u^2+g^2)^{-1}-1]^{\frac{1}{2}}. \tag{5}$$

Then ω is uniquely defined by

$$\cos\omega=-(u\beta+g)/2 \tag{6}$$

$$\sin\omega=\ (g\beta-u)/2\,. \tag{7}$$

If the point (u, g) is brought to the vicinity of a reflecting position and then u is varied and g held constant, the equations of motion for the various elements of the 'linkage' can be obtained by differentiation. $\dot{Y}$ is the angular velocity of the counter, $\dot{\omega}$ the angular velocity of the crystal and also the angular velocity of the reciprocal lattice as it rotates about Q (since the reciprocal lattice is always linked to the crystal). $\dot{u}$ is the linear velocity of the point (u, g).

Upon differentiating (3) and (4), respectively, we obtain

$$dY/d\omega=1+\sin\omega/\sin(Y-\omega) \tag{8}$$

and

$$dY/du=2u/[(u^2+g^2)\beta]\,. \tag{9}$$

We have from (9)

$$\dot{Y}=2u\dot{u}/[(u^2+g^2)\beta] \tag{10}$$

and from (8), making substitutions from (3), (7) and (10),

$$\dot{\omega}=\dot{u}(g+u\beta^{-1})/(u^2+g^2)\,. \tag{11}$$

3. Counter drive linkage

In our earliest approach to this problem, the linkage mechanism shown schematically in Fig. 2 was developed. In this arrangement a crystal goniometer support (not shown) is mounted on the crystal support spindle C. Spindle C is rigidly affixed to gear E which rotates about axis O (normal to plane of sketch) when driven by idler gear F. The counter detector drive wheel H, on which is fixed the counter detector support arm B with adjustable pin P, rotates counterclockwise, increasing the angle Y. When H is rotated, pin P constrains the motion of slotted driving bar A about the axis J, controlling the crystal angular change ω. The rotation of bar A about axis J is transferred to gear I. Screw L normal to slotted bar A is rigidly attached to gear I. By turning knob K, the base of bar A can be translated along L providing the adjustment to change g. (An adjustment provides for positioning the pin P in positions intermediate to the points P, N. This adjustment is not used in the equi-inclination scheme; it is required for n-level normal beam recording or generalized inclination techniques.) When aligned, the reciprocal lattice line $\overline{PP'}$ of Fig. 1(*b*) is parallel to the slotted bar A.

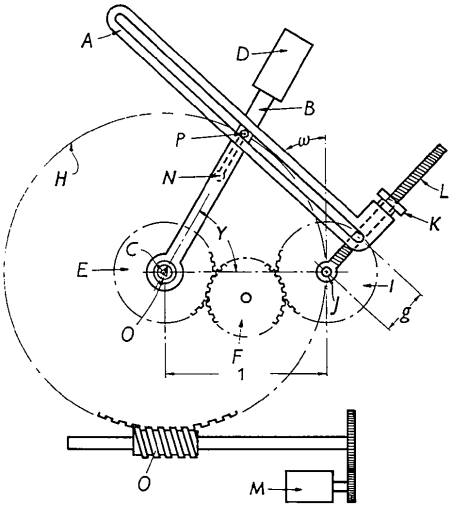

Fig. 2. Schematic of counter drive linkage mechanism, a mechanical analog for the construction of Fig. 1(*b*).

The counter detector D is attached to the support arm B by means of an extensible arc (not shown) which is adjusted to the equi-inclination angle for n-level data collection. The counter drive wheel H is driven by means of the worm Q which is driven by the motor M.

An automatic diffractometer, Fig. 3, utilizing this linkage mechanism has been constructed and is being used to reinvestigate the crystal structure of topaz. A full description of this automatic diffractometer, PAILRED I, (Philips Automatic Indexing Linear Reciprocal-Lattice Exploring Diffractometer) will be given elsewhere.

It should be noted that the linkage shown in Fig. 3 is the mirror image of the schematic of Fig. 2. In the pilot model shown, the automatic diffractometer has

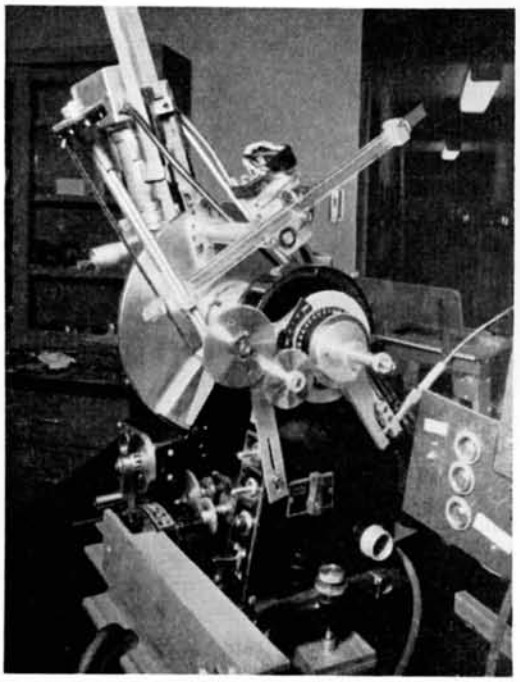

Fig. 3. Early version of PAILRED I, an automatic diffractometer based upon the linkage mechanism shown in Fig. 2. The instrument coded by means of a notched lucite bar (seen at upper right) has been developed from standard 'Norelco' powder diffractometer. The angular scale seen at the right is the 'ω' scale, and the cable drive seen at the extreme right is for independent rotation of the crystal through a small fixed angular range.

been constructed using a standard powder diffractometer as a base. Although this experimental instrument suffices for an *ad hoc* demonstration of the counter drive linkage, it should be noted that the instrument bears no resemblance to that which could be considered a satisfactorily designed single crystal diffractometer, nor should it be construed that the various appendages retained from its previous usage as a powder diffractometer are pertinent to its present application. Fig. 3 is primarily presented to show an actual execution of the counter drive linkage and also to illustrate the instrument used to obtain the data of Fig. 5.

The essential characteristics of the counter drive mechanism can be summarized as follows: The angular velocity of the counter $\dot{Y}$ is constant. The range of the mechanism allows an uninterrupted exploration along the line $\overline{PP'}$ from the point $(-(4-g^2)^{\frac{1}{2}}, g)$ to the point $(0, g)$. If for convenience we let $\dot{Y}=-1$, we have in this range

$$\dot{\omega}=-(g\beta+u)/(2u) \tag{12}$$

and

$$\dot{u}=-\beta(u^2+g^2)/(2u)\,. \tag{13}$$

If the exploration is initiated at the maximum counter angle, the crystal velocity is initially one-half the angular velocity of the counter. The crystal decelerates as its angular velocity increases and the angular velocity becomes zero at the point of tangency where $u=-g\beta=(2g-g^2)^{\frac{1}{2}}$. The angular velocity $\dot{\omega}$ continues to increase (as the crystal rotation direction is reversed) until it becomes infinite at the terminal point of exploration, $u=0$. The angular velocity $\dot{\omega}$ is plotted as a function of u for several values of g in Figs. 4(a) and 4(b). The linear velocity $\dot{u}$ increases monotonically in the course of the exploration. Consequently, traverse of reflections near the origin of the reciprocal lattice is executed in less time than that of the more distant reflections. The linear velocity $\dot{u}$ is plotted against u for 3 values of g in Fig. 4(c).

When this mechanism is used to accumulate reflec-

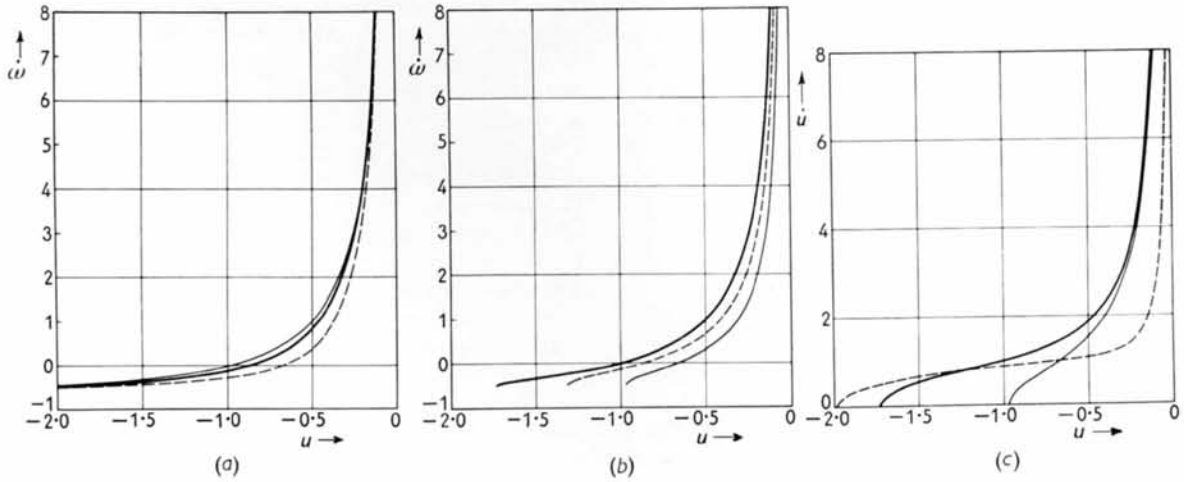

Fig. 4. Kinematic relations for counter drive linkage. ($\dot{Y}$ constant) (a) $\dot{\omega}$ is plotted as a function of u for $g=0{\cdot}25$, dashed line; $g=0{\cdot}50$, heavy solid line; and $g=0{\cdot}75$, light solid line. (b) $\dot{\omega}$ is plotted as a function of u for $g=1{\cdot}00$, heavy solid line; $g=1{\cdot}50$, dashed line; and $g=1{\cdot}75$, light line. (c) $\dot{\omega}$ is plotted as a function of u for $g=0{\cdot}25$, dashed line; $g=1{\cdot}00$, heavy solid line; and $g=1{\cdot}75$, light solid line.

tion data for a complete level, g is incremented (after a specific line is explored) to adjust the mechanism for the exploration of the next adjacent parallel reciprocal lattice line. Since the g increment is proportional to the reciprocal repeat distance in the direction $\overline{QQ'}$, the incrementation is uniform from line to line and can easily be accomplished automatically. Knob K (Fig. 2), for example, can be turned by means of a synchronous motor controlled by an accurate timing mechanism which rotates knob K for a fixed time interval, which has been adjusted to be proportional to the required g-increment. In this manner after exploring along a specified reciprocal lattice line, the counter can be automatically returned to the maximum angle and the screw L (Fig. 2) advanced to position the mechanism to explore the next adjacent parallel line. Thus, for one alignment (i.e., fixing screw L normal to the set of reciprocal lattice lines parallel to $\overline{PP'}$) of the crystal relative to the linkage mechanism, $\frac{1}{4}$ of the entire level within the total circle of reflection (radius $2\overline{OQ}$) can be automatically explored in one continuous uninterrupted operation.

To utilize this linkage mechanism in an automatic diffractometer it is necessary to take into account the variation of $\dot{\omega}$ in the exploration along $\overline{PP'}$. Since the integrated intensity is defined as the energy entering the counter as the crystal is rotated at constant angular velocity, the implication of Fig. 4(a), (b), is that integrated intensity recordings made for reflections at different values of (u, g) are not comparable. Moreover, for small values of u the variation of $\dot{\omega}$ in the course of scanning through one reflection may be sufficient to significantly affect the interpretation of the recorded integrated intensity. To bring the recorded intensities on a comparable scale, each integrated intensity record could be corrected by multiplying the observed intensity by a special 'Lorentz' factor, $|2u/(g\beta+u)|$, obtained from equation (12). If the reflection intensity is to be measured by means of a continuous ratemeter recording of the reflection line profiles and the integrated intensity inferred from the observed peak heights, the variation of $\dot{\omega}$ will cause a 'recording error' in the display of each peak height. The recording error has been studied by Parrish (1956), who showed that for line profiles of similar shape the product of the scanning speed, $(\dot{\omega})$, and ratemeter time constant determines the percentage of ideal peak height lost in the display due to the inertia of the ratemeter recording pen. This recording error can be corrected in principle by means of an analog device which varies the 'time constant' of the ratemeter inversely with $\dot{\omega}$. An alternative procedure that is more satisfactory has been utilized in PAILRED I. An automatic stepping assembly is used to arrest the motion of the counter during the exploration whenever a reciprocal lattice point site is reached. By means of this device, the speed of exploration can be increased in the region where no reflections occur and a more uniform* recording error for all reflections maintained by moving the crystal independently when a reciprocal lattice point is encountered.

Unlike the Bond (1955) diffractometer in which the arrest of the counter is accomplished by electronic sensing of counts above a selected threshold, PAILRED I utilizes geometrical conditions. In Fig. 2, reciprocal lattice sites are at fixed equal increments along bar A. The stepping assembly can be understood with reference to Fig. 3. In Fig. 3, a notched bar incremented in steps proportional to the reciprocal lattice repeat is affixed parallel to bar A of Fig. 2. In the course of rapid exploration the counter is arrested when the microswitch which rides on the notched bar is activated by entering a notch. The activation of the microswitch causes an independent scan through a small fixed angular range at constant crystal angular velocity. In this manner the effect of the recording error is the same for all reflections, and the magnitude of angular velocity of the crystal during the integrated intensity scan is uniform. There are, of course, other devices that could be used in place of the notched bars.

In Fig. 5(a) the results of a continuous ratemeter exploration and scan along the (02l) reciprocal lattice line of topaz are shown. The tracing at the right was obtained using monochromatized Mo $K\alpha$ radiation (50 kVP. 20 mA.) rotating the counter at $\dot{Y} = -1°$ per min. At the left, the tracing of the lower orders of (02l) was obtained under the same conditions except that $\dot{Y}$ was $-\frac{1}{4}°$ per min. The time constant of the ratemeter was 3 sec. in both cases. The extended and severely distorted profile of the (026) reflection results from the reversing of scanning directions and slow scanning speed in this vicinity which is the region where the (02l) line is tangent to the circle of reflection. The scanning speed for the (026) reflection in the tracing on the right is $\dot{\omega} = +0{\cdot}077°$ per min., and at the adjacent (027) reflection $\dot{\omega} = -0{\cdot}076°$ per min. The vicinity of tangency is easily identified since reflection profiles of orders greater than (026) show the $K\alpha_2$ component on the high Y angle side, whereas reflection profiles for orders less than (027) show the α_2 component on the low angle side.

The effect of the recording error mentioned above is evident upon comparing corresponding profiles of the same reflection. Thus, for example, the peak height of the (022) reflection seen on the left is more than twice the peak height of the (022) seen on the right. This is expected since the recording error is more pronounced for the right (022) owing to the faster scanning speed (the scanning speeds are $\dot{\omega} = 0{\cdot}890°$ per min. for the (022) on the left and $\dot{\omega} = 3{\cdot}560°$ per min. for the (022) on the right, respectively). Incidentally, a comparison of these peak heights reveals a serious error which can arise by injudicious inference of integrated

* We assume that the shapes of the reflection profiles are sufficiently similar at all diffraction angles so that the effect of profile shape on recording error can be ignored.

intensities from peak heights. Although the left (022) peak height is only twice the right (022) peak height, the integrated intensities are in fact in the ratio of 4 to 1 (because of the relative scanning speeds). An even greater error would be manifest if the integrated intensities of the left and right (025) reflections were inferred from the peak heights since for the (025) reflections the peak heights are in the ratio 9:6. Also, a comparison of the (025) reflections indicates that the recording error is significant even at slow scanning speeds. The scanning speeds of the (025) reflections are respectively $\dot{\omega}=0{\cdot}081°$ per min. (left) and $\dot{\omega}=0{\cdot}323°$ per min. (right).

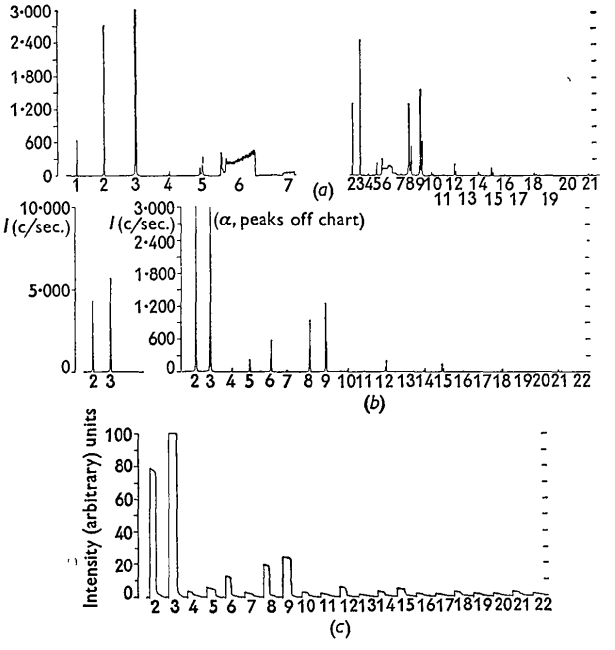

Fig. 5. Various displays obtained with PAILRED I. (*a*) Continuous scan along the reciprocal lattice line (02*l*) shown as detected with counter velocity $\dot{Y}=-1°$/min. on the left and with counter velocity $\dot{Y}=-\frac{1}{4}°$/min. on the right. The abscissa scale is $°Y$; the number beneath each profile is the l index of the line. The ordinate scale is intensity in counts per sec. (*b*) The reciprocal lattice line (02*l*) as explored and scanned with automatic stepping assembly. Each profile was scanned for seven minutes at the rate of $\dot{\omega}=\pm\frac{1}{2}°$/min. (Alternate lines were scanned in opposite directions.) The background was counted at the termination of each reflection scan for 73 sec. The record of the background count is visible only for lower order lines where the background count is significantly higher than base (zero count) line. The exploration was conducted at $\dot{Y}=-20°$/min. See text for details. The two lowest order lines were repeated (at left) at a scale factor for which full scale deflection = 10,000 counts/sec. (*c*) The same sequence as in (*b*) displaying the accumulated count for each reflection. The 'saw teeth' appearing between the reflection '*S*' curves are the background counts accumulated for 73 sec.

In Fig. 5(*b*) the same (02*l*) line is shown as scanned with the automatic stepping assembly. Under similar experimental conditions as above, the linkage was employed to bring the counter to successive reciprocal lattice sites, but the scan at each reflection was effected by independently rotating the crystal at constant speed $|\dot{\omega}|=\frac{1}{2}°$ per min. As is evident from Fig. 5(*b*), alternate reflections were scanned in opposite directions, i.e., for all reflections with l index odd $\dot{\omega}=-\frac{1}{2}°$ per min. and for l index even $\dot{\omega}=\frac{1}{2}°$ per min. (Alternating the sense of scan obviated backsetting the crystal after each scan.) The sequence of events that were executed in obtaining Fig. 5(*b*) was as follows: The crystal orientation was initially offset 1·75° from the position which would align the (02*l*) reciprocal lattice line to conform to equation (3), and the counter detector was brought to $Y=136°$. The automatic operation was initiated by causing the counter to rotate at $\dot{Y}=-20°$ per min. and operating the ratemeter. In the time interval during which the counter was in motion, the ratemeter was reset and consequently recorded zero counts. Upon reaching the angular (Y) position corresponding to a reflection site, the motion of the counter was arrested. With the counter stationary, the reset of the ratemeter was removed allowing the recording of counts as the crystal was rotated for seven minutes. After seven minutes the crystal motion was arrested and the ratemeter reset for five seconds. With both counter and crystal stationary, a record of the background count was made. The background count was sampled for 73 seconds. After recording the background, the ratemeter was reset and the next cycle initiated, i.e., the counter was rotated again at $-20°$ per min., and this procedure was repeated.

Because of the low background count as seen from the scales shown in Fig. 5(*b*), the portions of the tracing that were recorded during the intervals when the ratemeter was in the state of being reset are not clearly discernible in Fig. 5(*b*). The same automation scheme was used to obtain the tracing shown in Fig. 5(*c*), except that the ratemeter records the integrated or accumulated intensity. The time constant for the tracing of Fig. 5(*b*) was 3 sec., and that for Fig. 5(*c*) was 10 sec. The reset positions of the tracing in Fig. 5(*c*) are clearly visible; these are the line segments at zero count appearing between the '*S*' curves and triangles. If the line segments representing 'reset' time are added and the resulting length compared to the length of the entire tracing of Fig. 5(*c*), the ratio of time spent productively at each reflection site can be compared to the time used to explore the line and separate the data displayed. By actual calculation the 'non-productive' time spent in exploring the (02*l*) line for 20 reflections was 8 min., and the productive time (scanning and measuring background) spent was 23·3 min.

The line profiles seen in Fig. 5(*b*) can be compared with corresponding line profiles of Fig. 5(*a*). The disparity between peak heights and the widths of the profile are due to variation in scanning speed. The lines seen in Fig. 5(*b*) are all subject to a uniform re-

cording error. The information lost because of the high scanning speed of the low order lines in Fig. 5(*a*) is revealed by the relatively high peak heights seen for these same lines in Fig. 5(*b*).

The tracing of Fig. 5(*c*) shows the principle advantage of the discontinuous scan. Here the accumulated intensity count is registered; the height of the S curve represents the total number of counts detected in the scan of a fixed angular range. The 'S' shape of the curve results from the $K\alpha_1-\alpha_2$ resolution of the line profile being integrated. The net integrated intensity for a given reflection is the difference between the height of the S curve and ψ times the altitude of the right triangle adjacent to the curve which represents the accumulated background count. ψ is the ratio of time spent on the reflection scan to the time spent counting background, in this case $\psi=5{\cdot}7$.

To expedite data reduction, the information obtained in Fig. 5(*c*) has also been obtained utilizing an electronic counter which displays the number of counts accumulated in the scan of each reflection and the number of counts accumulated in the measure of the background. This decimal information is preserved by means of an accessory which prints out the information. Another accessory stores the information in code by punching the data on paper tape. The tape code has been designed so that the intensity data can be directly processed and interpreted on an electronic calculator.

Although a satisfactory automatic diffractometer has been constructed using the counter drive linkage, there are certain disadvantages that should be cited. (1) The mechanical stability of the linkage is not satisfactory in the vicinity of $u=0$ because $|\dot{\omega}|\gg|\dot{Y}|$ in this region. As a consequence, the 'ratio of transmission' defined as $|\dot{Y}/\dot{\omega}|$ is small. The small ratio of transmission causes a large reactive torque in the output link (which changes ω), thereby straining the linkage. To avoid the instability in the vicinity of $u=0$, a practical design would require a more massive linkage, but this in turn would be 'overdesigning' for most of the range of the mechanism. (2) When used to accumulate zonal (or level) data, the range with one alignment of the crystal with this linkage is limited to $\frac{1}{4}$ of the total circle of reflection.

4. Crystal drive mechanism

The scheme for providing a continuous analog solution for equation (3) by utilizing the crystal drive mechanism has been developed independently by Mathiesen (1958), and an account of the method has been given by him. Here the features of this mechanism are merely summarized so a comparison can be made with the other mechanisms described.

Using Mathiesen's arrangement, the range traversible in an uninterrupted exploration along a given line (g constant) is from $(-(2g-g^2)^{\frac{1}{2}}, g)$ to $((4-g^2)^{\frac{1}{2}}, g)$. If we let the constant angular velocity of the crystal, $\dot{\omega}$, equal -1, we have

$$\dot{Y}=-2u/(g\beta+u) \tag{14}$$

and

$$\dot{u}=-(u^2+g^2)/(g+u\beta^{-1})\,. \tag{15}$$

$\dot{Y}$ and $\dot{u}$ are plotted against u for several values of g in Figs. 6(*a*), (*b*), (*c*). Note that if the exploration is initiated at the maximum counter angle, $\dot{Y}$ is initially twice $\dot{\omega}$, analogous to the case of the counter drive mechanism. As the counter moves to lower angles, $\dot{Y}$ increases (becoming less negative) to zero at the minimum counter angle where $u=0$. $\dot{Y}$ continues to increase in the region $-(2g-g^2)^{\frac{1}{2}}\leq u\leq 0$ and becomes infinite where $u=-(2g-g^2)^{\frac{1}{2}}$, the point of tangency.

The advantage of this mechanism is the uniform recording error for all reflections. However, this advantage does not obviate the need for an automatic stepping assembly particularly when integrated intensities are to be registered, since the intensity of a particular reflection must be distinguished from the intensity of non-Bragg scatter near the reflection site, i.e., a truncation device is needed so that only the intensity within a fixed angular range of reflection is

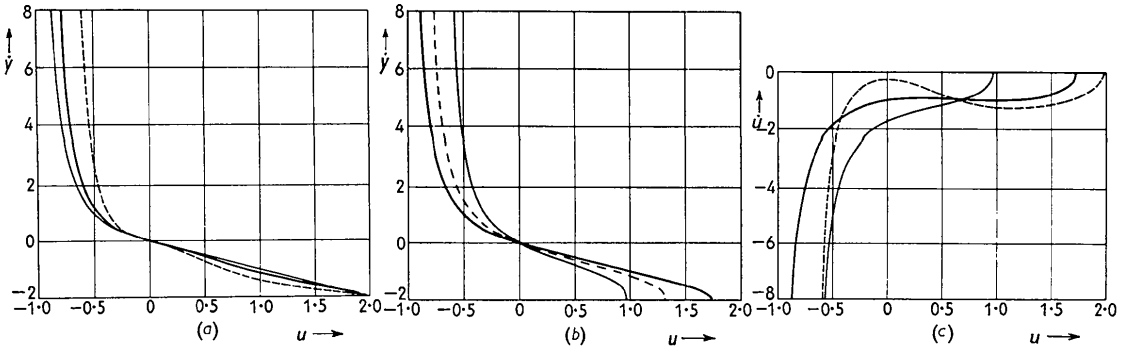

Fig. 6. Kinematic relations for crystal drive linkage. ($\dot{\omega}$ constant) (*a*) $\dot{Y}$ is plotted as a function of u for $g=0{\cdot}25$, dashed line; $g=0{\cdot}50$, heavy solid line; and $g=0{\cdot}75$, light solid line. (*b*) $\dot{Y}$ is plotted as a function of u for $g=1{\cdot}00$, heavy solid line; $g=1{\cdot}50$, dashed line; and $g=1{\cdot}75$, light solid line. (*c*) $\dot{u}$ is plotted as a function of u for $g=0{\cdot}25$, dashed line; $g=1{\cdot}00$, heavy solid line; and $g=1{\cdot}75$, light solid line.

recorded. Moreover it is still desirable to traverse rapidly from reflection site to reflection site. Another advantage to this method (which was not mentioned in Mathiesen's paper) is the possibility of scanning several levels simultaneously (using the normal beam Weissenberg geometry) using n sets of counter detectors, linkages and recorders, one for each level, with the linkages connected in tandem.

The primary mechanical disadvantage of this scheme is the infinite velocity of $\dot{Y}$ at $u=-(2g-g^2)^{\frac{1}{2}}$. As in the counter drive method where $\dot{\omega}$ is infinite at $u=0$, simple electromechanical devices can be used to limit the range of these mechanisms and in this way avoid the infinite velocities. When used to accumulate zonal (or level) data, it is easy to show that the range with one alignment of the crystal is limited to $\frac{3}{8}$ of the total circle of reflection.

5. Point drive mechanism

An improved mechanism that incorporates the best features of the previously described mechanisms and yet circumvents their fundamental limitations has been devised and is shown schematically in Fig. 7. The mechanism of Fig. 7 is a direct mechanical analog of the geometry of Fig. 1(*b*). In Fig. 7, nut A is welded to shaft B. Shaft B is free to rotate in a bearing drilled in counter detector arm C. Detector arm C terminates in a sleeve which houses shaft L and rotates about axis D. Nut A rides on worm E and can be linearly displaced along the length of carriage F when the motor $M1$ is energized. Carriage F is rigidly connected to nut G in such a manner as to maintain carriage F always normal to worm I for any position of nut G on worm I. Worm I is supported in bearing H which is rigidly connected to shaft J by means of yoke K. The rotation of shaft J is transferred by means of gears (not shown) to shaft L which supports the crystal on axis D. Motor $M2$, when energized rotates worm I causing nut G to advance away from bearing H. The X-ray beam entering from the left in the plane of $\overline{RR'}$ and $\overline{DO}$ intersects the crystal at O; the counter angle is shown by Y and the crystal angle by ω. The analog of the displacement of the reciprocal lattice line, g, is the distance between the centers of shaft J and nut G. The analog of the reciprocal lattice line to be scanned is the line segment along the entire worm E.

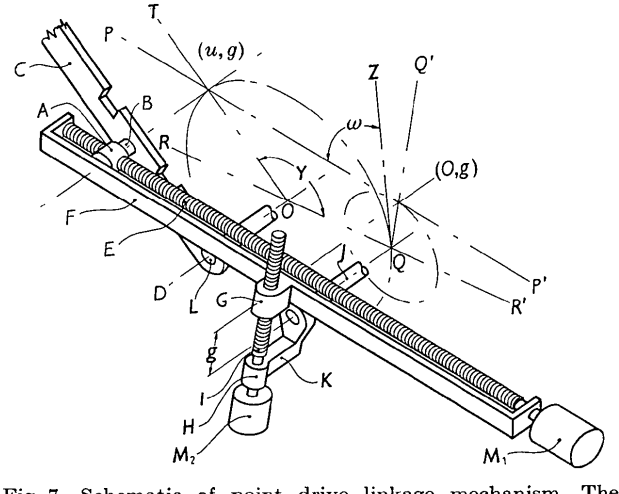

Fig. 7. Schematic of point drive linkage mechanism. The mechanism is a mechanical analog of the construction of Fig. 1(*b*) which is here shown again in perspective. See text for description of the various parts of the mechanism.

The range scanned with the point drive mechanism is $(-(4-g^2)^{\frac{1}{2}}, (4-g^2)^{\frac{1}{2}})$ (i.e., the entire line included within the total circle of reflection). In this mechanism, $\dot{u}$, the linear velocity of the point u is held constant. If we let $\dot{u}=+1$, we have for the angular velocity of the counter

$$\dot{Y}=+2u/[(u^2+g^2)\beta] \tag{16}$$

and the angular velocity of the crystal

$$\dot{\omega}=+(g+u\beta^{-1})/(u^2+g^2)\,. \tag{17}$$

In Figs. 8(*a*), (*b*), $\dot{Y}$ and $\dot{\omega}$ are plotted against u for several values of g. The motions are interpreted in the same manner as in the case of the previously described linkage mechanisms.

It is clear from equations (16) and (17) that neither the angular velocity of crystal or counter becomes infinite except for the singular point $(u, g)=(0, 0)$, at which the crystal velocity becomes infinite.

An automatic diffractometer, PAILRED II, has been designed on the basis of this mechanism and will be described in detail when its construction is completed and its operational efficiency evaluated. With this new instrument it will be possible to scan automatically all reflections of a given level within $\frac{1}{2}$ the circle of reflection. By merely rotating the crystal goniometer support 180°, the remaining half of the level will be obtained without further attention. The constancy of $\dot{u}$ permits simplification of the design of automation compared to PAILRED I. Firstly, the automatic stepping device need not be contained in the instrument because the 'stepping' required can be accomplished by energizing synchronous motors for fixed time intervals instead of moving microswitches on incrementation bars. These can easily be arranged to operate by remote control. Secondly, the absence of infinite angular velocities (except at the blind spot $u=g=0$) makes the direction of exploration immaterial. This enables the alternation of exploration directions for adjacent lines and permits thereby a considerable saving of exploration time.

6. Conclusion

Three mechanisms have been described which provide for the continuous analog solution of the tracking equation (3). These mechanisms differ in the range accessible in an uninterrupted scan along a specified reciprocal lattice line, the linear velocity of scan $\dot{u}$,

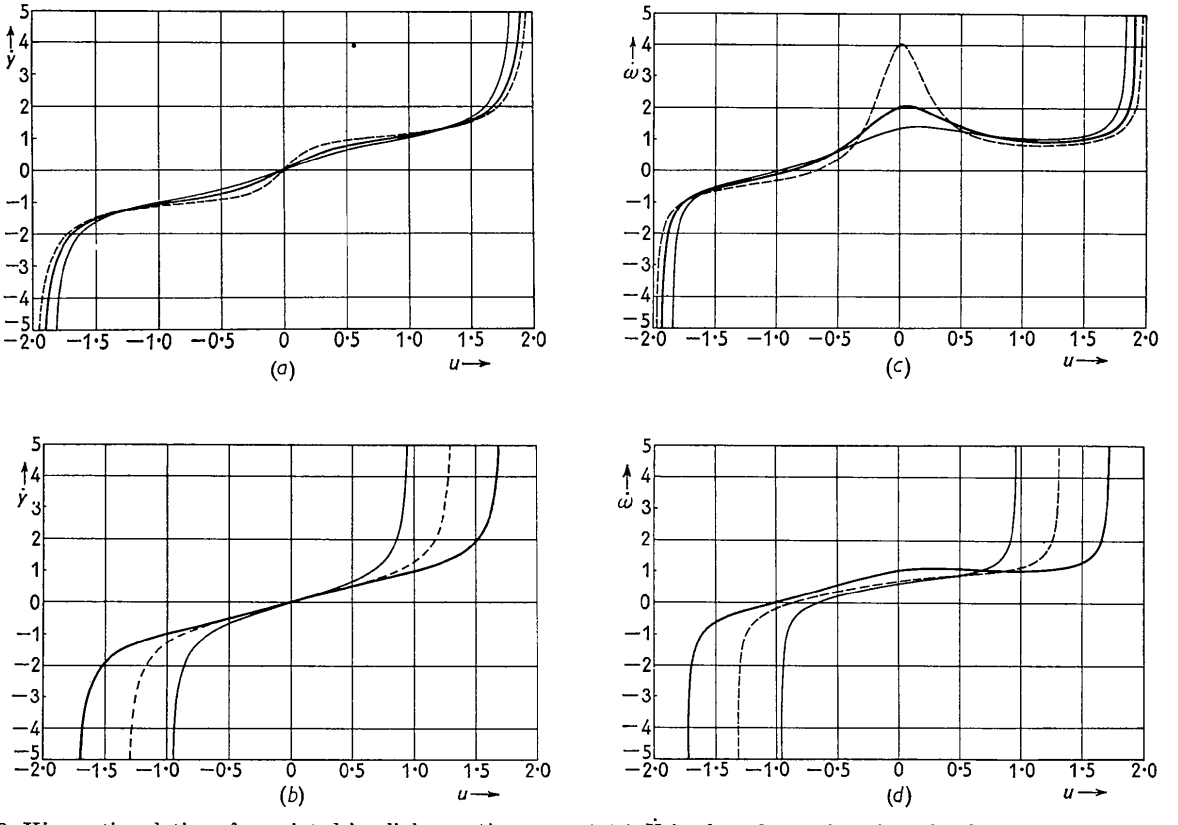

Fig. 8. Kinematic relations for point drive linkage. ($\dot{u}$ constant) (*a*) $\dot{Y}$ is plotted as a function of u for $g=0{\cdot}25$, dashed line; $g=0{\cdot}50$, heavy solid line; and $g=0{\cdot}75$, light solid line. (*b*) $\dot{Y}$ is plotted as a function of u for $g=1{\cdot}00$, heavy solid line; $g=1{\cdot}50$, dashed line; and $g=1{\cdot}75$, light solid line. (*c*) $\dot{\omega}$ is plotted as a function of u for $g=0{\cdot}25$, dashed line; $g=0{\cdot}50$, heavy solid line; and $g=0{\cdot}75$, light solid line. (*d*) $\dot{\omega}$ is plotted as a function of u for $g=1{\cdot}00$, heavy solid line; $g=1{\cdot}50$, dashed line; and $g=1{\cdot}75$, light solid line.

Table 1. *Comparison of linkage mechanisms*

	Counter drive	Crystal drive	Point drive
Range in u (g constant)	$(-(4-g^2)^{\frac{1}{2}},\ 0)$	$(-(2g-g^2)^{\frac{1}{2}},\ (4-g^2)^{\frac{1}{2}})$	$(-(4-g^2)^{\frac{1}{2}},\ (4-g^2)^{\frac{1}{2}})$
$\dot{u}$	$\frac{(u^2+g^2)\beta}{2u}\dot{Y}$	$\frac{u^2+g^2}{g+u\beta^{-1}}\dot{\omega}$	Constant
$\dot{\omega}$	$\frac{(g\beta+u)}{2u}\dot{Y}$	Constant	$\frac{g+u\beta^{-1}}{u^2+g^2}\dot{u}$
$\dot{Y}$	Constant	$\frac{2u}{(g\beta+u)}\dot{\omega}$	$\frac{2u}{(u^2+g^2)\beta}$

the angular velocity of the counter $\dot{Y}$, and the angular velocity of the crystal $\dot{\omega}$. The results are summarized in Table 1.

These linkage mechanisms provide a general scanning procedure for the optimum employment of counter detectors in single crystal diffractometry, and their use obviates the need for independent laborious and time-consuming calculation of crystal and counter setting angles. The kinematic relations summarized in Table 1 and Figs. 4, 6 and 8 provide the information to make the appropriate velocity corrections in reducing the intensity data to structure factors; these also illustrate the tolerances required in the precise mechanical execution of the mechanisms.

The mode of surveying the reciprocal lattice with these mechanisms is particularly advantageous in temperature diffuse scattering studies because the distribution of diffuse scattering in any specified direction in the reciprocal lattice can be quickly ascertained and displayed in a ratemeter tracing.

The authors acknowledge the encouragement, ad-

vice and assistance given by Dr William Parrish and the extensive calculations performed by Miss Marian Mack, both of this laboratory.

References

BOND, W. L. (1955). *Acta Cryst.* **8**, 741.

BUERGER, M. J. (1942). *X-ray Crystallography*. New York: Wiley.

CLIFTON, D. F., FULLER, AARON & MCLACHLAN, D. (1951). *Rev. Sci. Instrum.* **22**, 1024.

COCHRAN, W. (1950). *Acta Cryst.* **3**, 268.

EVANS, H. T. (1953). *Rev. Sci. Instrum.* **24**, 156.

HIRSHFELD, F. L. & SCHMIDT, G. M. J. (1953). *Bull. Res. Coun. Israel* (*Weizmann Memorial Issue*), **3**, 37.

JAMES, R. W. (1950). *The Optical Principles of the Diffraction of X-rays*. London: Bell.

LANGDON, F. & FRAZER, B. C. (1959). *Rev. Sci. Instrum.* **30**, 997.

LONSDALE, K. (1948). *Acta Cryst.* **1**, 12.

MATHIESEN, A. MCL. (1958). *Acta Cryst.* **11**, 433.

OKAYA, Y., SAITO, Y. & PEPINSKY, R. (1955). *Phys. Rev.* **98**, 1857.

PARRISH, W. (1956). *Philips Tech. Rev.* **17**, 206.

PARRISH, W., HAMACHER, E. A. & LOWITZSCH, K. (1954). *Philips Tech. Rev.* **16**, 123.

PARRISH, W. & KOHLER, T. R. (1956). *Rev. Sci. Instrum.* **27**, 795.

PEPINSKY, R., DRENCK, K. & DIAMANT, H. (1959). *Abstract for Stockholm Meetings*, Commission on Crystallographic Apparatus, International Union of Crystallography, June 9–12, 1959.

Acta Cryst. (1960). **13**, 215

The Crystal Structure of Acepleiadylene

BY A. W. HANSON

Division of Pure Physics, National Research Council, Ottawa, Canada

(*Received* 24 *June* 1959)

The crystal of acepleiadylene is monoclinic, probably $P2_1/a$,

$$a = 11{\cdot}59,\ b = 11{\cdot}48,\ c = 7{\cdot}93\ \text{Å},\ \beta = 100{\cdot}2°,\ Z = 4\ .$$

The structure was determined by inspection of a three-dimensional Patterson synthesis, and refined with the aid of three-dimensional Fourier syntheses. The structure is disordered, the average asymmetric unit consisting of two molecules related by an approximate symmetry centre, and occupying roughly the same space. The structure is very similar to that of pyrene; the distance between adjacent parallel molecules is 3·44 Å.

Introduction

Acepleiadylene is a non-alternant hydrocarbon first synthesized by Boekelheide & Vick in 1956. The compound has recently been the subject of theoretical and experimental investigation, including some speculation about the crystal structure (Pullman, Pullman,

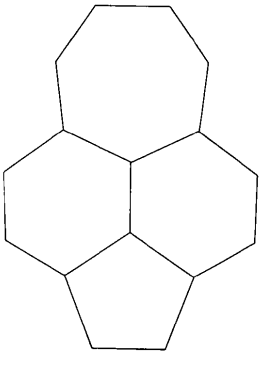

Berthier & Pontis, 1952; Sidman, 1956*a*, *b*; Pitt, Petro & Smyth, 1957). X-ray analysis was therefore undertaken with the object of discovering the nature of the packing in the crystalline state and the stereochemistry of the molecule, including bond lengths. It will be seen that this object was realized only in part.

Experimental details

The crystals of acepleiadylene available for examination were red, granular and opaque. From an examination of precession photographs it was found that the crystal was monoclinic, probably $P2_1/a$, with

$$a = 11{\cdot}59 \pm 0{\cdot}04,\ b = 11{\cdot}48 \pm 0{\cdot}04,\ c = 7{\cdot}93 \pm 0{\cdot}03\ \text{Å};\quad \beta = 100{\cdot}2°.$$

Also,

D_x (calculated density) = 1·30 g.cm.$^{-3}$ ($Z = 4$).
D_o (measured density) = 1·29 g.cm.$^{-3}$.
$\mu = 7{\cdot}1$ cm.$^{-1}$ (Cu $K\alpha$). $\mu = 23{\cdot}1$ cm.$^{-1}$ (Cr $K\alpha$).
Melting point 161 °C.

Fielding & Schneider (1959) report a very small